Acta Mech 225, 1685–1698 (2014)
DOI 10.1007/s00707-013-1023-y

M. Rebouah · G. Chagnon

Permanent set and stress-softening constitutive equation applied to rubber-like materials and soft tissues

Received: 23 May 2013 / Revised: 19 August 2013 / Published online: 10 November 2013

Abstract Many rubber-like materials present a phenomenon known as Mullins effect. It is characterized by a difference of behavior between the first and second loadings and by a permanent set after a first loading. Moreover, this phenomenon induces anisotropy in an initially isotropic material. A new constitutive equation is proposed in this paper. It relies on the decomposition of the macromolecular network into two parts: chains related together and chains related to fillers. The first part is modeled by a simple hyperelastic constitutive equation, whereas the second one is described by an evolution function introduced in the hyperelastic strain energy. It contributes to describe both the anisotropic stress softening and the permanent set. The model is finally extended to soft tissues' mechanical behavior that present also stress softening but with an initially anisotropic behavior. The two models are successfully fitted and compared to experimental data.

1 Introduction

Despite many different studies, the accurate prediction of rubber-like materials' mechanical behavior is still an open issue. These materials have the great capacity to endure large deformations and cyclic conditions. Nevertheless, they present also highly nonlinear phenomena that make difficult to truly model them. In this paper, it is proposed to focus on three main phenomena. The first phenomenon is the stress softening [1] that occurs between the first and second loadings. This stress softening can be imputed to chain microstructure rearrangements in the material [2] and depends on the maximal strain reached. Indeed, once the previous maximum strain is exceeded, the loading curve comes back on the primary curve [3–6]. The second phenomenon often observed for rubber-like materials is the permanent set. This phenomenon is characterized by a residual strain that depends on the maximal strain reached and of the composition of the material, i.e., the amount of fillers [7–9]. The third phenomenon is the induced anisotropy by the stress softening. It has been observed that the stress softening of a material is maximal for a second loading along the direction of the first loading and minimum for a second loading along the orthogonal direction to the first loading direction [8,10–14]. These three phenomena are known as the Mullins effect.

For several years, many authors developed models to predict the behavior of rubber-like materials. The first models were principally isotropic [15–19]. Later, some constitutive equations taking into account permanent set were developed. Dorfmann and Ogden [20] proposed a model by means of the pseudo-elasticity, which is an isotropic model able to take into account the stress softening and the permanent set. This model is one of the most employed and was implemented into a finite element code. The eight-chain model [21], with its analytical form more easily usable than other chain models, stimulates the development of micro-physically motivated models. The micro-spherical models first proposed by [22–24] and then by [8,11,25,26] are constitutive equations that

M. Rebouah · G. Chagnon (✉)
Universite de Grenoble/CNRS/TIMC-IMAG UMR 5525, Grenoble 38041, France
E-mail: gregory.chagnon@imag.fr
Tel.: +334-56-520086
Fax: +334-56-520044

allow to describe hyperelasticity, viscoelasticity, and plasticity. But it also permits to describe the induced anisotropy by stress softening by means of this repartition of directions in space. The space repartition permits to use different evolution functions or identical evolution functions that would evolve differently. It is to note that according to the spatial discretization used some unphysical anisotropy can be induced by the model used [27,28]. But few models are able to take into account stress softening, permanent set, and induced anisotropy of a material. Recently, Rickaby and Scott [29] developed a constitutive equation to describe stress softening, permanent set, and relaxation behavior but limited to equibiaxial loading. Itskov et al. [30] also proposed recently a model to take into account anisotropic softening and permanent set by means of a pseudo-strain energy. Moreover, Merckel et al. [8,31] developed a tridimensional model describing the permanent set and the stress softening, but considered then as independent phenomena.

In the last few years, it was observed that the understanding of the behavior of soft tissues gets improved [32–35], and thus, the multiplication of model appears. It is well known that soft tissues present a similar behavior to rubber-like materials. Thus, soft tissues present also a stress softening. It was observed, for example, for arteries [36,37], venas [38], vaginal tissues [39], esophageal [40], etc. Inspired by the rubber-like materials phenomenological models [20], several authors proposed pseudo-elastic models adapted to soft tissues [41,42]. Phenomenological models based on 3D generalization model were also proposed, and Alastrue et al. [43] readapted the exponential model and the 8 chains model. Nevertheless, soft tissues present also an initial anisotropic behavior due to their structure. Most of the soft tissues are composed of a matrix reinforced by fibers; thus, the models built for them are based on an initially anisotropic constitutive equation that depends on the orientation of the fibers [40,44–48]. Some models were adapted to take into account the stress softening and the permanent set [37,49]. Generally, the stress softening is treated by considering that it only occurs in the fibers and not in the matrix.

Most of the existing models do not treat simultaneously the three phenomena of the Mullins effect. A new constitutive equation is developed here by means of a micro-spherical model, to take into account the stress softening with the permanent set and the induced anisotropy for rubber-like materials by using a formulation with strain invariant and by considering these phenomena as independent. This model is then adapted to soft tissues by adding an initial anisotropy with fibers. In this way, in Sect. 2 an experimental study lead on a filled silicone rubber is presented highlighting the stress softening, the induced anisotropy, and the permanent set. In Sect. 3, constitutive equations are developed to take into account these effects for rubber-like materials. Section 4 presents a successful comparison of the model with the experimental data. Finally, Sect. 5 presents the extension of the constitutive equation to soft tissues, and the results are compared to experimental data from the literature.

2 Experimental data on silicone rubber

2.1 Materials

Two materials are used for this study, an initially isotropic one, a silicone rubber and, an initially anisotropic one, an ovine vena cava [50]. The silicone rubber used is a heat-cured silicone (HCS) also called Hot Temperature Vulcanization (HTV) which contains 30 % of fillers (silica). This filled silicone rubber is vulcanized with a peroxyde starter. A plate of 185 mm length, 170 mm width, and 2.5 mm thick is molded and vulcanized under an increasing pressure (0.1–0.5 MPa) and a temperature 180 °C. No experimental study is lead on the soft tissues. The experimental data are used from Peña et Doblaré [50].

2.2 Classical tensile tests

Tensile tests were realized on samples of 15 mm length, 2.5 mm width, and 2.5 mm thick cut from the molded rectangular plate. First, the influence of the strain rate is evaluated. Cyclic tensile tests up to $\lambda = 2.5$ (λ represents the actual length of a sample over its initial length) were performed at different strain rates: 0.025, 0.167, 1, 1.667 s^{-1}. For these small variations of the strain rate, there is no significant influence on the mechanical behavior of rubber-like material. For the study, it is thus chosen to perform all the following tests at a strain rate of 1 s^{-1}. Second, silicone specimens were submitted to cyclic loading up to a fixed stretch. Each of the specimens was subjected to two loading unloading cycles up to $\lambda = 2$. After completion of the second unloading cycle, each specimen was then loaded up to a stretch of $\lambda = 2.5$. No recovery time was allowed

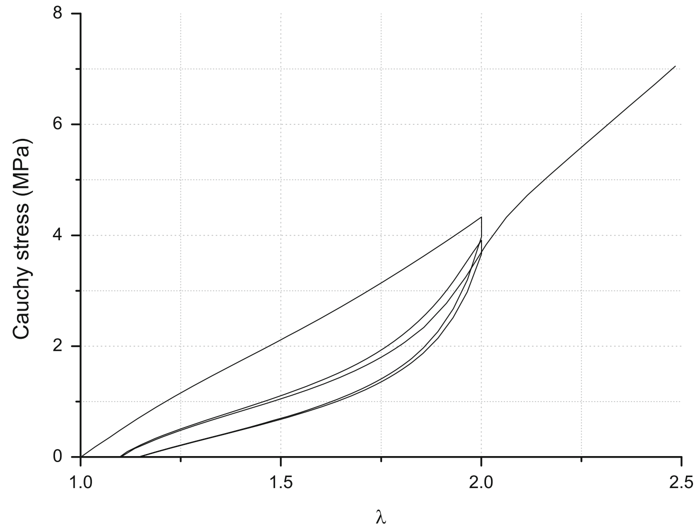

Fig. 1 Cyclic tensile test on HTV silicone at a strain rate of 1 s^{-1}

during the two loading–unloading cycles. The results of one test can be observed in Fig. 1. The stress softening and the permanent set can be observed as an hysteretic behavior, which is not taken into account in this study.

2.3 Induced anisotropy by the Mullins effect

In this section, it is proposed to highlight the induced anisotropy by the Mullins effect in the HTV silicone rubber. First, a large sample of silicone is prepared for a pure shear test, and it is presented in Fig. 2a. This sample of 40 mm length, 15 mm width, and 2 mm thick is submitted to a cyclic tensile test up to $\lambda = 2$. This test is performed at a strain rate of 1 s^{-1}. Next, several samples are cut from this sample along different orientations ($\alpha = 0°$, $\alpha = 25°$, $\alpha = 45°$, $\alpha = 90°$) compared to the first tensile direction as illustrated in Fig. 2b. Four new samples of 15 mm length, 2.5 mm width, and 2 mm thick are obtained. Each specimen is subjected to a loading–unloading cycle up to $\lambda = 2.5$ at a strain rate of 1 s^{-1}.

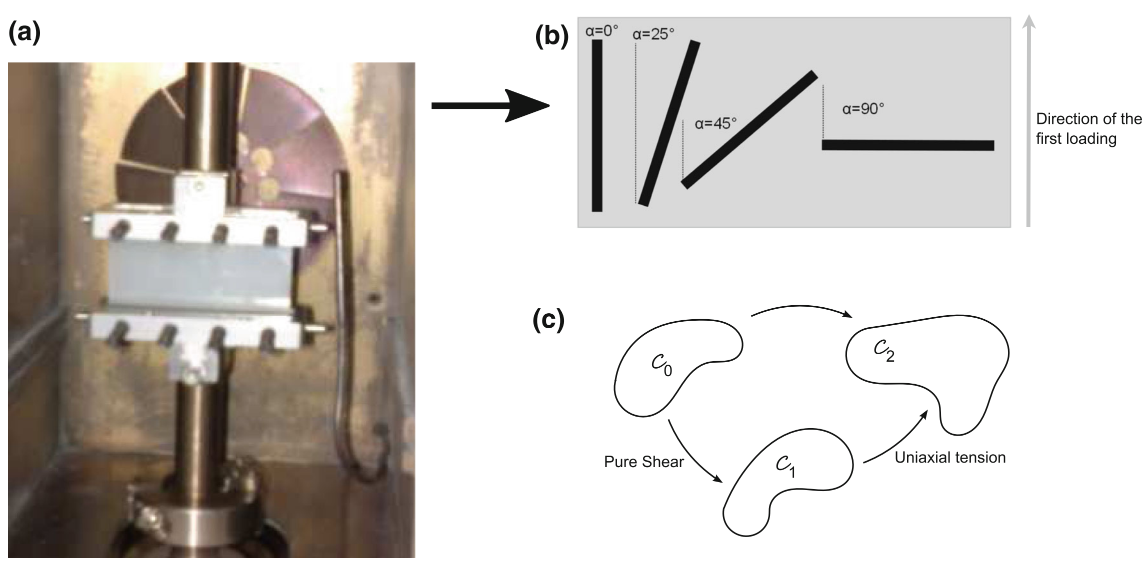

Fig. 2 Experimental device used to highlight induced anisotropy by Mullins effect (**a**) pure shear test, **b** geometry of the cut specimens inside the pure shear specimen, **c** definition of the configurations, (C_0) initial configuration, (C_1) configuration after the pure shear test, (C_2) configuration after the pure shear and tensile tests

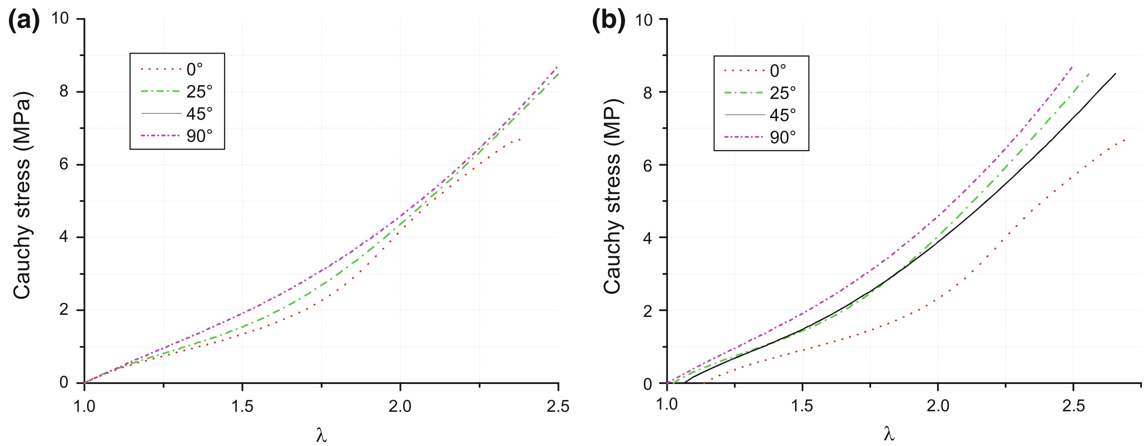

Fig. 3 Influence of the angle between the first and second loadings on the stress softening compared to (**a**) configuration C_1, i.e., without taking into account the permanent set after the first loading and (**b**) compared to configuration C_0, i.e., by taking into account the permanent set after the first loading

The mechanical test realized and described in Fig. 2 can be studied in different configurations (cf. Fig. 2c). The first configuration C_0 is the initial configuration of the sample (before pure shear test). The C_1 configuration is the intermediary configuration (after pure shear test), and C_2 is the final configuration where the four samples cut according to different orientations from the pure shear test sample are submitted to a tensile test. By means of these tests, several observations can be done. First, the influence of the orientation of the samples is highlighted in Fig. 3a. For this representation, it is considered that the initial configuration is C_1 and not C_0 (cf. Fig. 2c). The reference configuration is thus considered after the pure shear test that means that the stress softening is studied without initial permanent set induced by the pure shear test. This allows to focus on the influence of the orientation. It is observed that for an orientation of $\alpha = 90°$ the material has the same behavior as a first loading (i.e., behavior similar to a virgin material). For an orientation of $\alpha = 0°$, the mechanical behavior is a classical second loading without change of direction. The intermediary orientations $\alpha = 25°$ and $\alpha = 45°$ present a behavior between a first and second loadings; the stress softening is more important for the orientation of $\alpha = 25°$ than for the orientation of $\alpha = 45°$, but the two curves come back on the same point on the first loading curve. These conclusions are the same as previously shown on a RTV silicone [51].

It is also proposed to represent these four tensile tests by taking into account the complete history of the material i.e., compared to the initial configuration C_0 (cf. Fig. 2c), i.e., the permanent set generated by the pure shear test is now taken into account. The results are presented in Fig. 3b. The same stress softening as in Fig. 3a is observed, and also the amount of permanent set endured lasting the pure shear test for the different samples. It is observed that the more the orientation is close to the first loading direction, the more the permanent set is important. Indeed, for an orientation of $\alpha = 0°$, it can be observed that an initial permanent set (due to the pure shear test) of $\lambda_{\text{resid}} = 1.136$ and at the opposite for the sample cut at $\alpha = 90°$ the initial permanent set is null. These results are similar to those obtained in the literature [51].

3 Constitutive equation

3.1 General form

Recently, Rebouah et al. [26] developed a constitutive equation written with strain invariants to predict the anisotropic stress softening in filled silicone rubbers but without permanent set. Based on the idea of Govindjee [53], the strain energy density of the material $\mathscr{W}_{\text{silicone}}$ is additively decomposed into two parts: one that represents the strain energy of the chains linked to filler $\mathscr{W}_{cf}$ and an other part that represents the strain energy of the chains linked to other chains $\mathscr{W}_{cc}$. The total strain energy density is thus $\mathscr{W}_{\text{silicone}} = \mathscr{W}_{cc} + \mathscr{W}_{cf}$. Rebouah et al. [26] considered that only $\mathscr{W}_{cf}$ can evolve with the Mullins effect. In our approach, it is also proposed to describe the permanent set by means of $\mathscr{W}_{cf}$. Thus, $\mathscr{W}_{cf}$ is represented by an anisotropic strain energy function that can record the deformation history of the material. Any micro-sphere model defined by a spatial direction repartition $\mathbf{A}^{(i)}$ can be chosen. The dilatation in each direction is defined by means of $I_4{}^{(i)} = \mathbf{A}^{(i)}.\mathbf{C}\mathbf{A}^{(i)}$ where

$\mathbf{C}$ is the right Cauchy–Green deformation tensor, defined by $\mathbf{C} = \mathbf{F}^T\mathbf{F}$, and $\mathbf{F}$ is the deformation gradient. The general form of the model is as follows:

$$\mathscr{W}_{\text{silicone}} = \mathscr{W}_{cc}(I_1, I_2) + \sum_{i=1}^{n} \omega^{(i)} \mathscr{F}^{(i)} \mathscr{W}_{cf}^{(i)}(I_4^{(i)}). \tag{1}$$

$\mathscr{W}_{cc}$ is an hyperelastic energy density, and I_1, I_2 are the first and second strain invariants of $\mathbf{C}$. $\mathscr{W}_{cf}^{(i)}$ is the hyperelastic strain energy associated with each direction, and $\omega^{(i)}$ represents the weight of each direction. They are given by Bazant and Oh [54], and $\mathscr{F}^{(i)}$ is the Mullins effect evolution function. The HTV silicone does not present strain hardening; thus, it is decided to use a strain energy that is not presenting a large increase in slope with deformation. The Mooney [15] strain energy function is chosen for $\mathscr{W}_{cc}$, and a particular form is proposed for $\mathscr{W}_{cf}$. Previously, [26] the quadratic equation proposed by Kaliske et al. [52] was used. Nevertheless, for this material, this equation presents a stress hardening too important to represent the considered material, and thus, a function with a few hardening is used:

$$\text{if} \quad I_4{}^{(i)} \geq 1 \quad \mathscr{W}_{cf}^{(i)}(I_4^{(i)}) = \tfrac{K}{2} \int \sqrt{\frac{I_4^{(i)} - 1}{I_4^{(i)}}} dI_4^{(i)} \quad \text{else} \quad 0 \tag{2}$$

where K is the only material parameter. It is to note that it is considered here that the strain energy in each direction is considered only in tension.

Rebouah et al. [26] proposed an evolution function which depends on the first and fourth invariants with only one material parameter η. The evolution function is the product of three terms. The first is an isotropic term which depends only on the first invariant and represents the global deformation of the material (similar to isotropic approaches); the second represents the maximal deformation of each direction of the material; and the third the triaxiality of the loading state. In this paper, it is proposed to adapt the constitutive equation to represent both stress softening and permanent set. For the HTV silicone rubber, the isotropic part is useless, and then, it is omitted here. The evolution of the stress softening is then different for this material; the powers of the two terms of the evolution function are changed and can be considered as parameters. The proposed function is as follows:

$$\mathscr{F}^{(i)} = 1 - \eta \left(\frac{I_{4\,\max}^{(i)} - I_4^{(i)}}{I_{4\,\max}^{(i)} - 1} \right)^{\beta} \left(\frac{I_{4\,\max}^{(i)}}{I_{4\,\max}} \right)^{\gamma}. \tag{3}$$

As proposed in the literature [55], the stress softening is described by the difference between the current strain and the maximum strain. The first term of the equation is the ratio of this difference between the current and undeformed states. The second term represents the triaxiality of the strain by the ratio of the strain in one direction compared to the maximum one. The powers assigned to each term must be chosen to represent at the best the mechanical behavior of the material and to avoid numerical problems. It is to note that these functions are phenomenological, and their form is not motivated by micro-mechanical observations.

The parameters η, β, and γ influence simultaneously the stress softening and the permanent set of the material. $I_{4\max}^{(i)}$ represents the maximal value of $I_4^{(i)}$ for the whole material history for each direction, and $I_{4\,\max}$ represents the maximal value of $I_4^{(i)}$ for the whole material history and all directions. To control the permanent set, a strong restriction proposed by Rebouah et al. [26] is suppressed here, and the evolution function $\mathscr{F}^{(i)}$ is allowed to become negative. That means that the zero stress of a direction is no longer sufficient for zero deformation but for a deformation depending on the parameter η. It is to note that the evolution function $\mathscr{F}^{(i)}$ depends on two different maximal values of the fourth invariant, i.e., in the considered direction, and for the whole material. Finally, the Cauchy stress is obtained by the following:

$$\sigma_{\text{silicone}} = \boldsymbol{\sigma}_{cc} + \boldsymbol{\sigma}_{cf} - p\mathbf{I} \tag{4}$$

where $\boldsymbol{\sigma}_{cc}$ is the part of the Cauchy stress that represents the chains linked to other chains and $\boldsymbol{\sigma}_{cf}$ the part of the Cauchy stress that represents the chains linked to fillers, expressed as follows:

$$\boldsymbol{\sigma}_{cc} = 2\mathbf{B}\frac{\partial W_{cc}}{\partial I_1} + 2\left(I_1\mathbf{B} - \mathbf{B}^2\right)\frac{\partial W_{cc}}{\partial I_2}, \tag{5}$$

$$\boldsymbol{\sigma}_{cf} = 2\sum_{i=1}^{42} \omega^{(i)} \mathscr{F}^{(i)} \frac{\partial W_{cf}}{\partial I_4^{(i)}}^{(i)} \mathbf{F}\mathbf{A}^{(i)} \otimes \mathbf{A}^{(i)} \mathbf{F}^T \tag{6}$$

where the 42 directions repartition proposed by Bazant and Oh [54] were chosen, in this study.

3.2 Validity of the model

It remains to verify that the presented model is in agreement with the requirements of thermodynamics (see e.g., Coleman and Gurtin [56]). If only isothermal processes are considered, the Clausius-Duhem inequality must be satisfied,

$$-\frac{\partial \mathscr{W}_{\text{silicone}}}{\partial I_{4\max}^{(i)}} \dot{I}_{4\max}^{(i)} \geq 0, \tag{7}$$

$$-\frac{\partial \mathscr{W}_{\text{silicone}}}{\partial I_{4\max}} \dot{I}_{4\max} \geq 0 \tag{8}$$

where $\dot{I}_{4\max}^{(i)} \geq 0$ and $\dot{I}_{4\max} \geq 0$ are the maximum deformation increase rates. By means of manipulations of Eqs. (7), (8), and (1), it can be easily established the next sufficient relations with the functions $\mathscr{F}^{(i)}$:

$$\frac{\partial \mathscr{F}^{(i)}}{\partial I_{4\max}^{(i)}} \leq 0 \quad \forall i, \tag{9}$$

$$\frac{\partial \mathscr{F}^{(i)}}{\partial I_{4\max}} \leq 0 \quad \forall i. \tag{10}$$

Considering the generic form of the evolution constitutive equation (3), it can be explicitly written that

$$\begin{aligned} \frac{\partial \mathscr{F}^{(i)}}{\partial I_{4\max}^{(i)}} = & -\eta\alpha \frac{\left(I_{4\max}^{(i)} - 1\right) - \left(I_{4\max}^{(i)} - I_4^{(i)}\right)}{\left(I_{4\max}^{(i)} - 1\right)^2} \left(\frac{I_{4\max}^{(i)} - I_4^{(i)}}{I_{4\max}^{(i)} - 1}\right)^{\beta-1} \left(\frac{I_{4\max}^{(i)}}{I_{4\max}}\right)^{\gamma} \\ & -\eta\beta \frac{1}{I_{4\max}} \left(\frac{I_{4\max}^{(i)} - I_4^{(i)}}{I_{4\max}^{(i)} - 1}\right)^{\beta} \left(\frac{I_{4\max}^{(i)}}{I_{4\max}}\right)^{\gamma-1} \end{aligned} \tag{11}$$

$$\frac{\partial \mathscr{F}^{(i)}}{\partial I_{4\max}} = -\eta\beta I_{4\max}^{(i)} \left(\frac{I_{4\max}^{(i)} - I_4^{(i)}}{I_{4\max}^{(i)} - 1}\right)^{\beta} \left(\frac{I_{4\max}^{(i)}}{I_{4\max}}\right)^{\gamma-1} \tag{12}$$

To verify Eqs. (9) and (10), the conditions to verify are $\alpha > 0,\ \beta > 0$, and $\left(I_{4\max}^{(i)} - 1\right) - \left(I_{4\max}^{(i)} - I_4^{(i)}\right) > 0$. This last condition is automatically verified if $I_4^{(i)} \geq 1$. It is verified for $I_4^{(i)} \leq 1$ by means of Eq. (1) as no energy is considered in compression that means that this term becomes 0.

4 Simulations of the model

To validate the model, it is proposed to compare its simulations to the different mechanical tests. The values of the material parameters were fitted on the different mechanical tests. The obtained values are as follows: $C_1 = 0.3$ MPa, $C_2 = 0.15$ MPa, $K = 1.6$ MPa, $\eta = 5,\ \beta = 0.5$, and $\gamma = 2.5$.

4.1 HTV on a tensile test

First, the cyclic tensile test presented in Fig. 1 is compared to the prediction of the model. The results obtained are illustrated in Fig. 4. These results are satisfactory since it can be observed that the Mullins effect and the permanent set are quite well described by the model.

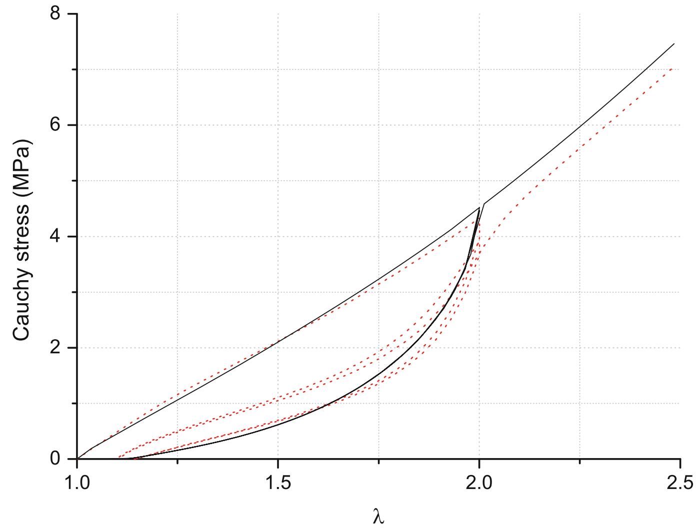

Fig. 4 Comparison of the prediction of the model (*full lines*) to experimental data (*dotted lines*)

4.2 HTV on a tensile test after a pure shear test

In this section, it is proposed to compare the model to the experimental results of the pure shear test followed by tensile tests according to different orientations. A comparison between the model and the tests is proposed in Fig. 5. It is to note that the first and second loadings (and thus the elongation) do not correspond to the same test. For each test, the definition of λ corresponds to the elongation in the tensile test direction whatever the experiment. Every simulated orientations present a similar behavior to the experimental results; thus, the same observation as the one made in paragraph 2.3 can be done. Furthermore, it is shown that the model is able to take well into account the induced anisotropy. Finally, for the curve at $\alpha = 25°$, it is observed that the second loading curve of the model presents a rupture of slope about $\lambda = 1.8$. This phenomenon is due to the discretization along the 42 directions of Bazant and Oh [54]. The problem is that the discretization in 42 directions creates a numerical anisotropy, as explained in the literature [27]. This phenomenon can be avoided with a full integration in space; nevertheless, the computational formulation become more complicated, and it becomes very time-consuming. Despite discretization problems, these results proved the ability of the model to take into account the induced anisotropy and the permanent set.

4.3 Analysis of the model simulations

In this part, it is proposed to analyze the evolution of the stress softening along the 42 spatial directions. The principal request directions during a cycling tensile test are observed along the direction of tension $\vec{x}$, where the maximal deformations are reached for different cycles until a maximal elongation of $\lambda = 1.5$, then $\lambda = 2$ and $\lambda = 2.5$. The 42 directions are represented in projection in the plane $(\vec{z}, \vec{y})$ in Fig. 6 as [22]. It is to note that many directions have the same angle with the $\vec{x}$ direction. They are summarized by the definition of 4 circles.

The stress σ_{xx} corresponds to the stress in the tensile direction. It is by construction the tensorial sum of stresses along the 42 directions [54]. The more a direction is closer from direction $\vec{x}$, the more its contribution to σ_{xx} is important. All the directions that belong to a same circle provide the same contribution in the case of uniaxial tension in direction $\vec{x}$. Thus, for clarity of the figure, only one direction per circle is presented. The stress strain behavior of each direction is presented in Fig. 7. It appears that the most loaded direction is direction 1, which is consistent since it corresponds to the tensile direction $\vec{x}$. Nevertheless, it is observed that the directions which belong to the circle 3 (4-5-6-7) and to the circle 4 (18-19-20-21) endure also an important deformation and generate important stresses. It can also be observed that the directions which belong to the circle 2 (10-11-12-13-14-15-16-17) have very small influence, and the directions which belong to the circle 1 (2-3-8-9) are equal to zero as they are loaded only in compression. Besides direction 1, circles 3 and 4 present a negative part of the Cauchy stress during second loadings that means that these directions present a permanent

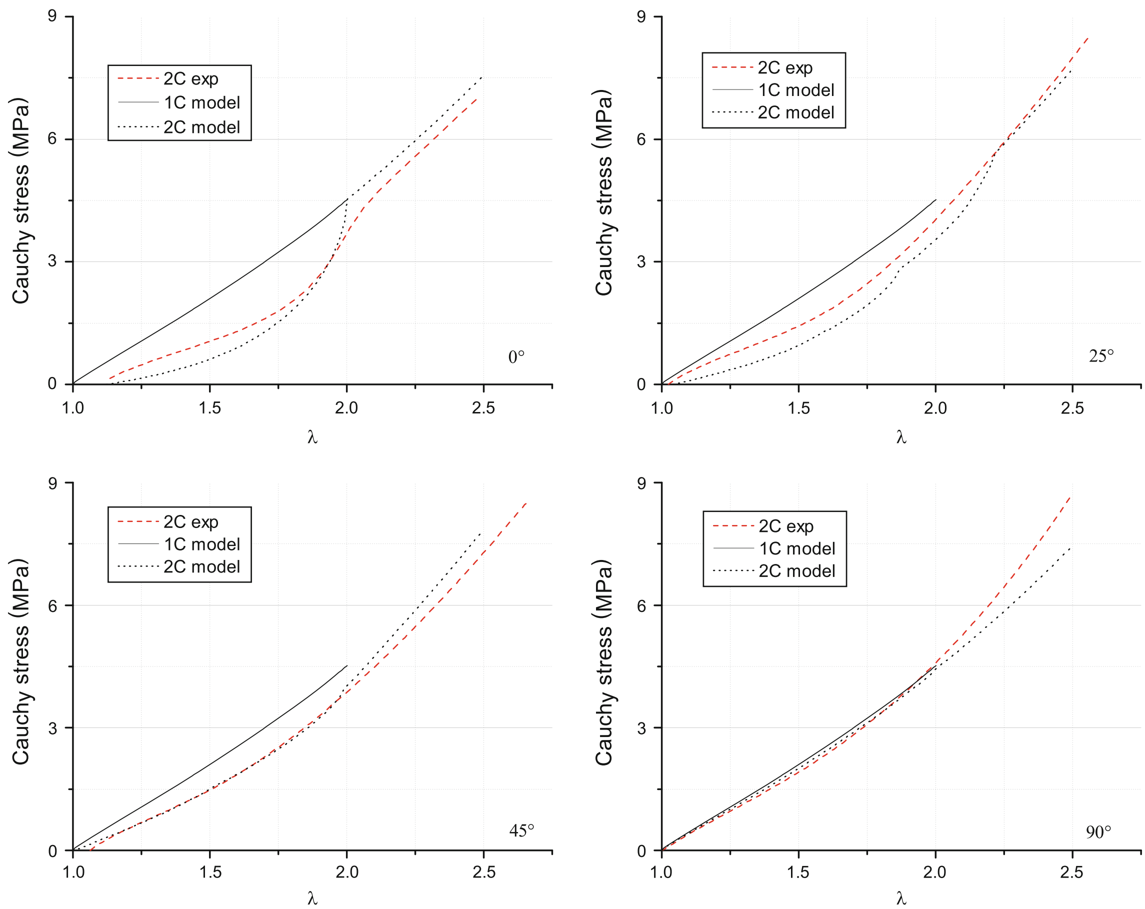

Fig. 5 Comparison with experimental oriented data and the model. The *black full lines* represent the theoretical first loading in uniaxial tension (1Cmodel); the *black dotted lines* represent the second loadings (i.e., the tensile test) for the different orientations (2Cmodel). The *red dashed lines* represent the experimental results for the different oriented samples of tensile tests after the pure shear test (2Cexp)

set. The directions that belong to circle 1 and 2 are still superior or equal to zero; thus, they do not present permanent set.

The evolution function generates a new equilibrium position, meaning that the zero stress state is no longer reached for zero deformation. This new equilibrium depends on the maximum deformation and is thus more important for directions close to direction $\vec{x}$. This is illustrated by Fig. 8. It is observed that along the direction 1, the circles 3 and 4, the evolution function becomes negative that means that the material presents a zero stress, and thus a permanent set. It is to note that the directions where the evolution function become negative are the same directions for which the stresses become negative and thus directions which generate permanent set. For this study, the 42 directions proposed by Bazant and Oh [54] were used; nevertheless, the other directions repartition proposed by the same author can also be used. It was proved that the results observed are identical, but they are not presented in the paper.

5 Adaptation of the constitutive equation to soft tissues

5.1 Adaptation of the model

It is proposed here to adapt the general form of the model previously described to non-initially isotropic materials, i.e., soft tissues. This anisotropy is imputed to the presence of fibers, often collagen [35], into the matrix of the tissue. In many soft tissues, there exist two main fibers orientations (the model will be developed for 2 directions, but the proposed principle would be the same for more directions). The orientation of these

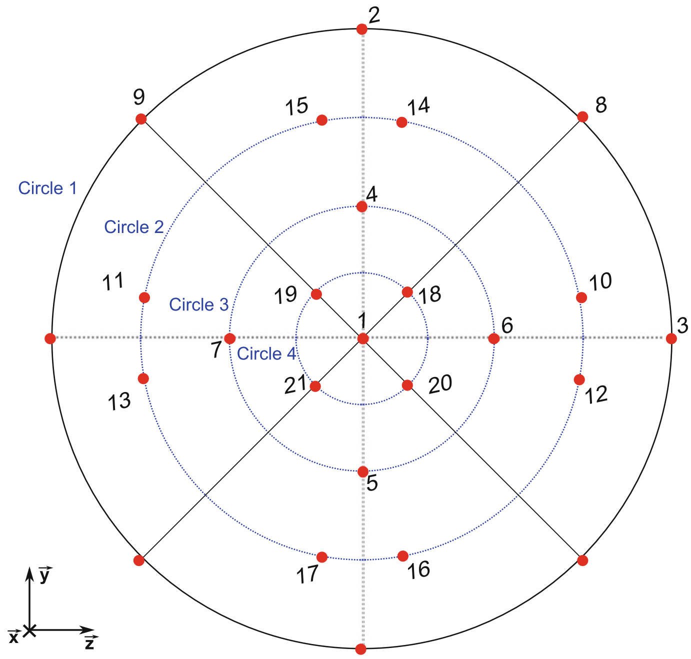

Fig. 6 Representation of the 42 Bazant and Oh directions in the plane $(\vec{z}, \vec{y})$

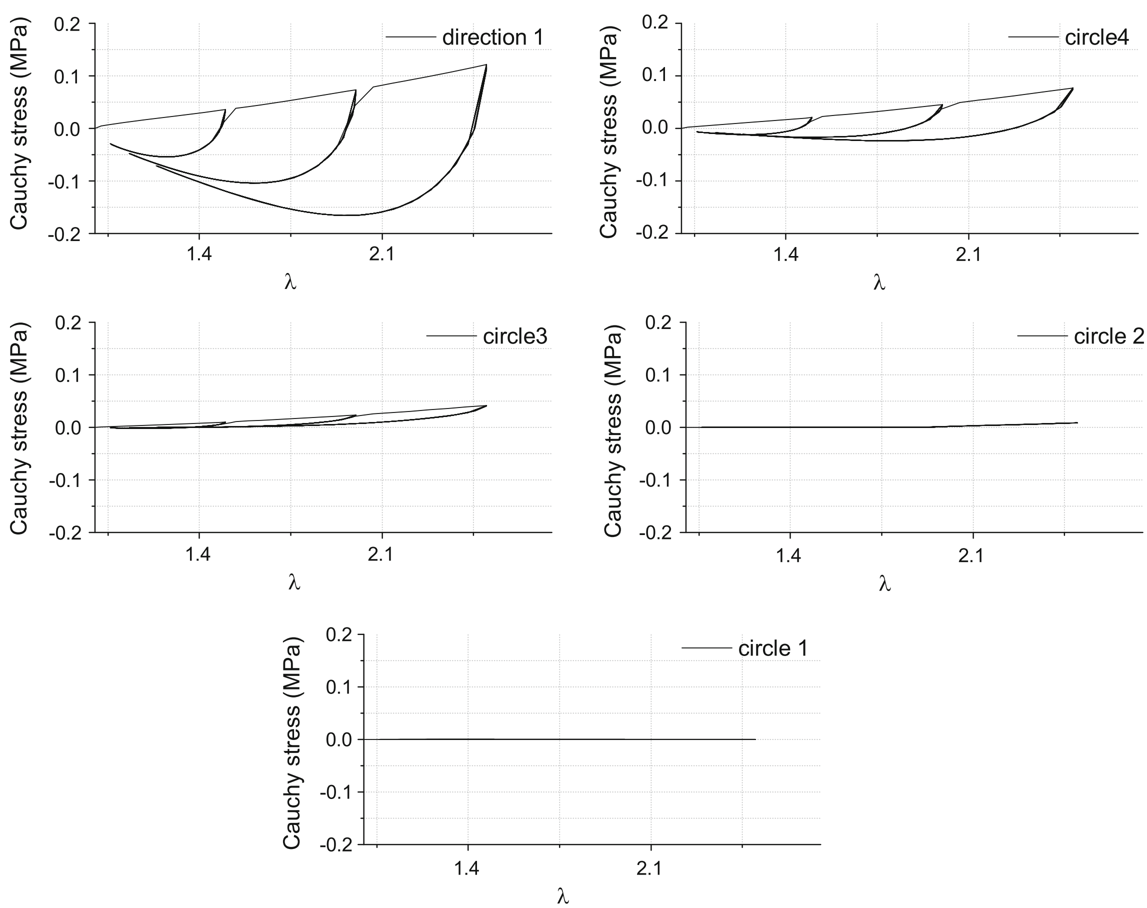

Fig. 7 Representation of the first component of the stress tensor (σ_{xx}) for cyclic tensile test up to $\lambda = 2.5$

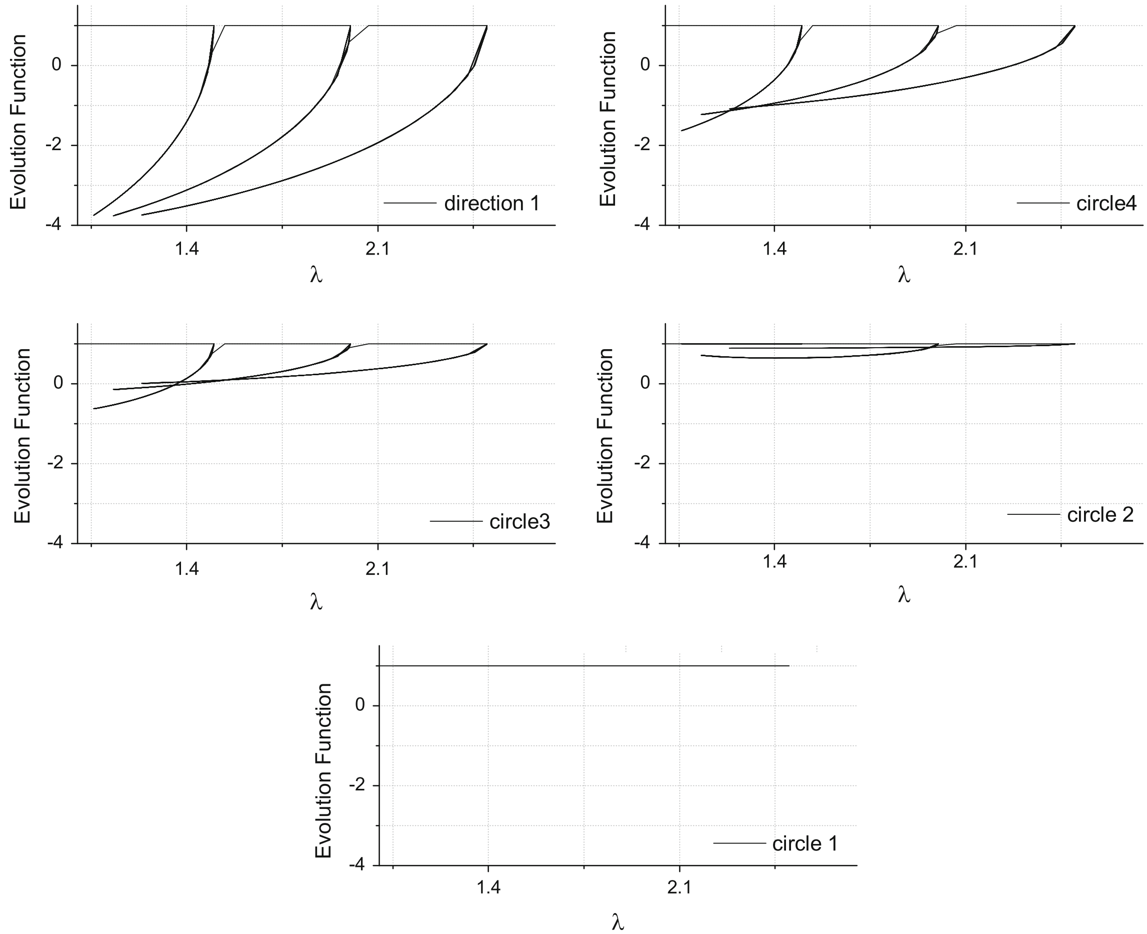

Fig. 8 Representation of the evolution function for cyclic tensile test up to $\lambda = 2.5$

fibers depends on the studied soft tissues [40,57–60]. As classically done in the literature, it is proposed to model the soft tissues mechanical behavior as the sum of three terms. The first part represents the behavior of the matrix, and the second and third parts represent respectively the mechanical behavior of the fibers oriented in the two directions,

$$\mathscr{W}_{\text{soft-tissue}} = \mathscr{W}_{\text{matrix}} + \mathscr{W}_{\text{fiber1}} + \mathscr{W}_{\text{fiber2}}. \tag{13}$$

It is also often assumed that the fibers can only endure tension, i.e., that no stress is generated in compression. The principle is to propose a strain energy that can simulate the stress softening both in the matrix and in the fibers. In the matrix, an initially isotropic strain energy is considered, which is similar to the one proposed for silicone rubbers in part 3. The same form is thus proposed,

$$\mathscr{W}_{\text{matrix}} = \mathscr{W}_{cc}(I_1) + \sum_{i=1}^{n} \omega^{(i)} \mathscr{F}^{(i)} \mathscr{W}_{cf}^{(i)}(I_4^{(i)}). \tag{14}$$

Different hyperelastic strain energies are used, as soft tissues present more strain hardening than silicone rubber. Classical strain energies are chosen for $\mathscr{W}_{cc}(I_1)$ [61,62] and $\mathscr{W}_{cf}^{(i)}$ [52], they are defined as follows:

$$\mathscr{W}_{cc}(I_1) = C_1 \exp\left(C_2(I_1 - 3)^2 - 1\right), \tag{15}$$

$$\mathscr{W}_{cf}^{(i)} = K(I_4^{(i)} - 1)^2 \tag{16}$$

where C_1, C_2, and K are material parameters. The evolution function $\mathscr{F}^{(i)}$ of the matrix is the same as the one used for silicone rubber model, described in Eq. (3).

The strain energy for fiber j is the product of an hyperelastic strain energy $\mathscr{W}_{\text{cf}-\text{fiber}_j}$ and an evolution function $\mathscr{F}_{\text{fiber}^{(j)}}$ to describe the Mullins effect:

$$\mathscr{W}_{\text{fiber1}} = \mathscr{F}_{\text{fiber}^{(j)}} . \mathscr{W}_{\text{cf}-\text{fiber}_j} . \tag{17}$$

The hyperelastic strain energy of each fiber is noted $\mathscr{W}_{\text{cf}-\text{fiber}_j}$ [63] and is expressed as follows:

$$\mathscr{W}_{\text{cf}-\text{fiber}_j} = \frac{K_f}{2} \exp(I_4^{(j)} - I_{4_0}^{(j)})^2. \tag{18}$$

K_f is a material parameter and $I_{4_0}^{(j)}$ matches to the value of $I_4^{(j)}$ for which the stress hardening of the material appears. Finally, due to the hypothesis of tension in the fiber, the evolution function is also adapted for the fibers, where only $I_4^{(j)}$ is necessary. A simplified form of the evolution function is used compared to the one used in Eq. (3). Indeed, for the fiber, only one direction is considered that means that the third term that took into account the triaxiality is not necessary. Only the second term is consistent,

$$\mathscr{F}_{\text{fiber}^{(j)}} = 1 - \eta_f \left(\frac{I_{4\,\text{max}}^{(j)} - I_4^{(j)}}{I_{4\,\text{max}}^{(j)} - 1} \right)^{\beta}, \tag{19}$$

where η_f and β are the material parameters which allow to take into account the stress softening and the permanent set of the fibers. It is to note that in this part it is considered that the material cannot endure compression; thus, the stress cannot become negative in any direction. Nevertheless, it generates the beginning of the permanent set for the material. This difference compared to the last model (for rubber-like materials) is due to the stress hardening of soft tissues which is very important, and thus, the evolution function must be adapted to correctly describe the phenomena.

5.2 Comparison with experimental data

To highlight the ability of the model to mimic soft tissues, it is proposed to compare it by means of the experimental data of Peña and Doblaré [50] considering first and second loadings at different maximum deformation in ovine vena cava during uniaxial tension. The orientation of the fibers was chosen at $\alpha = 45°$. These results were obtained for the following values of the different material parameters $C_1 = 0.28$ MPa; $C_2 = 0.16$ MPa; $K = 0.13$ MPa; $K_f = 0.5$ MPa; $\eta = 2$, $\eta_f = 5$ and $\beta = 2$.

As observed in Fig. 9 the experimental data obtained for loading–reloading cycles at different stretches are well described by the model. Figure 9a represents the theorical tensile test for a tensile test along the axial

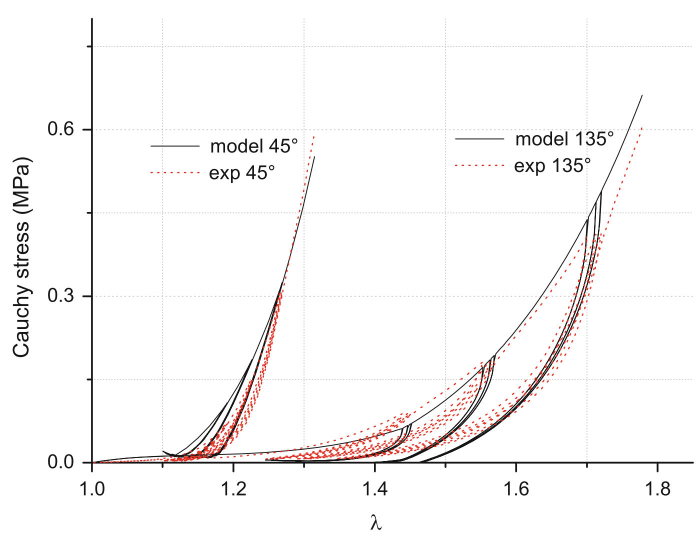

Fig. 9 Experimental data and comparison with the model for oriented sample of 45° and 135° in the tissue

direction for a value of $\alpha = 45°$, and Fig. 9b along the circumferential direction. For both tests, it is observed that the hyperelastic behavior, the stress softening, the permanent set, and the initial anisotropy are well taken into account. In this case, the induced anisotropy is not visible on the experimental data; nevertheless, the model can also take it into account.

6 Conclusion

As explained and shown in the present paper, a simple model is proposed here to take into account several effects of the Mullins effect. This model is adapted for both rubber-like materials and soft tissues. Compared to the literature [8,13], the major difference is that the permanent set and the stress softening are considered as correlated phenomena, and thus, the material parameters allow to represent simultaneously the stress softening and the permanent set. Due to the use of two different materials (HTV and soft tissues), different expressions were used for the strain energies and the evolution functions. Nevertheless, the discretization by a micro-sphere model represents well both the materials. Finally, by means of the extension of the model to soft tissues, the initial anisotropy of the materials can be taken into account independently of the induced anisotropy due to the stress softening. For both of these materials, the constitutive equations were successfully compared to experimental data to take into account simultaneously the stress softening of the material, the permanent set, the induced anisotropy, or the initial anisotropy of the material. Furthermore, due to the formulation in strain invariant of the constitutive equations, it can easily be implemented into a finite element code.

Acknowledgments The authors thank Professor Estefania Peña for helpful information on the experimental data of Peña and Doblaré [50]. This work is supported by the French National Research Agency Program ANR-12-BS09-0008-01 SAMBA (Silicone Architectured Membranes for Biomedical Applications)

References

1. Mullins, L.: Effect of stretching on the properties of rubber. Rubber Chem. Technol. **21**, 281–300 (1948)
2. Mullins, L.: Softening of rubber by deformation. Rubber Chem. Technol. **42**, 339–362 (1969)
3. Gurtin, M.E., Francis, E.C.: Simple rate-independent model for damage. J. Spacecraft **18**, 285–286 (1981)
4. Simo, J.C.: On a fully three-dimensional finite-strain viscoelastic damage model:Formulation and computational aspects. Comput. Meth. Appl. Mech. Eng. **60**, 153–173 (1987)
5. Miehe, C.: Discontinuous and continuous damage evolution in Ogden type large strain elastic materials. Eur. J. Mech. A/Solids **14**, 697–720 (1995)
6. Ogden, R.W. and Roxburgh, D.G.: An energy based model of the Mullins effect. In: Dorfmann, Muhr, (ed.) Constitutive Models for Rubber. I. A. A. Balkema (1999)
7. Ogden, R.W.: Mechanics of Rubberlike Solids. In: *XXI ICTAM*, Warsaw, Poland (2004)
8. Diani, J., Brieu, M., Vacherand, J.M.: A damage directional constitutive model for the Mullins effect with permanentset and induced anisotropy. Eur. J. Mech. A/Solids **25**, 483–496 (2006)
9. Merckel, Y., Diani, J., Roux, S., Brieu, M.: A simple framework for full-network hyperelasticity and anisotropic damage. J. Mech. Phys. Solids **59**, 75–88 (2011)
10. Laraba-Abbes, F., Ienny, P., Piques, R.: A new Taylor-made methodology for the mechanical behaviour analysis of rubber like materials: II. Application of the hyperelastic behaviour characterization of a carbon-black filled natural rubber vulcanizate. Polymer **44**, 821–840 (2003)
11. Itskov, M., Haberstroh, E., Ehret, A.E., Vohringer, M.C.: Experimental observation of the deformation induced anisotropy of the Mullins effect in rubber. KGK-Kautschuk Gummi Kunststoffe **59**, 93–96 (2006)
12. Machado, G., Favier, D., Chagnon, G.: Determination of membrane stress-strain full fields of bulge tests from SDIC measurements. Theory, validation and experimental results on a silicone elastomer. Exp. Mech. **52**, 865–880 (2012)
13. Merckel, Y., Brieu, M., Diani, J., Caillard, J.: A Mullins softening criterion for general loading conditions. J. Mech. Phys. Solids **60**, 1257–1264 (2012)
14. Dorfmann, A., Pancheri, F.: A constitutive model for the Mullins effect with changes in material symmetry. Int. J. Nonlinear Mech **47**, 874–887 (2012)
15. Mooney, M.: A theory of large elastic deformation. J. Appl. Phys. **11**, 582–592 (1940)
16. Treloar, L.R.G.: The elasticity of a network of long chain molecules (I and II). Trans. Faraday Soc. **39**:36–64; 241–246 (1943)
17. Ogden, R.W.: Large deformation isotropic elasticity—on the correlation of theory and experiment for incompressible rubber like solids. Proc. R. Soc. Lond. A **326**, 565–584 (1972)
18. Haines, D.W., Wilson, D.W.: Strain energy density function for rubber like materials. J. Mech. Phys. Solids **27**, 345–360 (1979)
19. Gent, A.N.: A new constitutive relation for rubber. Rubber Chem. Technol. **69**, 59–61 (1996)
20. Dorfmann, A., Ogden, R.W.: A constitutive model for the Mullins effect with permanent set in particule-reinforced rubber. Int. J. Solids Struct. **41**, 1855–1878 (2004)

21. Arruda, E.M., Boyce, M.C.: A three dimensional constitutive model for the large stretch behavior of rubber elastic materials. J. Mech. Phys. Solids **41**, 389–412 (1993)
22. Miehe, C., Göktepe, S., Lulei, F.: A micro-macro approach to rubber-like materials—Part I: The non-affine micro-sphere model of rubber elasticity. J. Mech. Phys. Solids **52**, 2617–2660 (2004)
23. Miehe, C., Göktepe, S.: A micro-macro approach to rubber-like materials. Part II: The micro-sphere model of finite rubber viscoelasticity. J. Mech. Phys. Solids **53**, 2231–2258 (2005)
24. Göktepe, S., Miehe, C.: A micro-macro approach to rubber-like materials. Part III: The micro-sphere model of anisotropic mullins-type damage. J. Mech. Phys. Solids **53**, 2259–2283 (2005)
25. Shariff, M.H.B.M.: An anisotropic model of the Mullins effect. J. Eng. Math. **56**, 415–435 (2006)
26. Rebouah, M., Machado, G., Chagnon, G., Favier, D.: Anisotropic Mullins stress softening of a deformed silicone holey plate. Mech. Res. Commun. **49**, 36–43 (2013)
27. Gillibert, J., Brieu, M., Diani, J.: Anisotropy of direction-based constitutive models for rubber-like materials. Int. J. Solids Struct. **47**, 640–646 (2010)
28. Ehret, A.E., Itskov, M., Schmid, H.: Numerical integration on the sphere and its effect on the material symmetry of constitutive equations- a comparative study. Int. J. Numer. Meth. Eng. **81**, 189–206 (2010)
29. Rickaby, S.R., Scott, N.H.: A model for the Mullins effect during multicyclic equibiaxial loading. Acta Mech. **224**, 1887–1900 (2013)
30. Itskov, M., Ehret, A., Kazakeviciute-Makovska, R., Weinhold, G.: A thermodynamically consistent phenomenological model of the anisotropic Mullins effect. ZAMM J. Appl. Math. Mech. **90**, 370–386 (2010)
31. Merckel, Y., Diani, J., Brieu, M., Caillard, J.: Constitutive modeling of the anisotropic behavior of Mullins softened filled rubbers. Mech. Mater. **57**, 30–41 (2013)
32. Lanir, Y.: A structural theory for the homogeneous biaxial stress-strain relationshipin flat collagenous tissues. J. Biomech. **12**, 423–436 (1979)
33. Lanir, Y.: Constitutive equations for fibous connective tissues. J. Biomech. **16**, 1–12 (1983)
34. Fung, Y.C.: Biomechanics, Mechanical Properties of Living Tissues. Springer, New York (1993)
35. Holzapfel, G.A.: Nonlinear Solid Mechanics—A Continuum Approach for Engineering. Wiley, NY (1993)
36. Vande Geest, J.P., Sacks, M.S., Vorp, D.A.: The effects of aneurysm on the biaxial mechanical behavior of human abdominal aorta. J. Biomech. **39**, 1324–1334 (2006)
37. Maher, E., Creane, A., Lally, C., Kelly, D.J.: An anisotropic inelastic constitutive model to describe stress softening and permanent deformation in arterial tissue. J. Mech. Behav. Biomed. Mater. **12**, 9–19 (2012)
38. Alastrué, V., Peña, E., Martinez, M.A., Doblaré, M.: Experimental study and constitutive modelling of the passive mechanical properties of the ovine infrarenal vena cava tissue. J. Biomech. **41**, 3038–3045 (2008)
39. Peña, E., Calvo, B., Martinez, M.A., Martins, P., Mascarenhas, T., Jorge, R.M.N., Ferreira, A., Doblaré, M.: Experimental study and constitutive modeling of the viscoelastic mechanical properties of the human prolapsed vaginal tissue. Biomech. Model. Mechanobiol. **9**, 35–44 (2010)
40. Natali, A.N., Carniel, E.L., Gregersen, H.: Biomechanical behaviour of oesophageal tissues: Material and structural configuration, experimental data and constitutive analysis. Med. Eng. Phys. **31**, 1056–1062 (2009)
41. Franceschini, G., Bigoni, D., Regitnig, P., Holzapfel, G.A.: Brain tissue deforms similarly to filled elastomers and follows consolidation theory. J. Mech. Phys. Solids **54**, 2592–2620 (2006)
42. Horgan, C.O., Saccomandi, G.: A new constitutive theory for fiber-reinforced incompressible nonlinearly elastic solids. J. Mech. Phys. Solids **53**, 1985–2015 (2005)
43. Alastrué, V., Martinez, M.A., Doblaré, M., Menzel, A.: Anisotropic microsphere-based finite elasticity applied to blood vessel modelling. J. Mech. Phys. Solids **57**, 178–203 (2009)
44. Balzani, D., Neff, P., Schroder, J., Holzapfel, G.A.: A polyconvex framework for soft biological tissues. Adjustement to experimental data. Int. J. Solids Struct. **43**, 6052–6070 (2006)
45. Nerurkar, N.L., Mauck, R.L., Elliott, D.M.: Modeling interlamellar interactions in angle-ply biologic laminates for annulus fibrosus tissue engineering. Biomech. Model. Mechanobiol. **10**, 973–984 (2011)
46. Calvo, B., Peña, E., Martinez, M.A., Doblaré, M.: An uncoupled directional damage model for fibred biological soft tissues. formulation and computational aspects. Int. J. Numer. Methods Eng. **69**, 2036–2057 (2007)
47. Caner, F.C., Carol, I.: Microplane constitutive model and computational framework for blood vessel tissue. J. Biomech. Eng. **128**, 419–427 (2006)
48. Driessen, N.J.B., B.C.V.C. and Baaiens, F.T.ens, F.P.T.: A structural constitutive model for collagenous cardiovascular tissues incorporating the angular fiber distribution. J. Biomech. Eng. **127**, 494–503 (2005)
49. Peña, E., Martins, P., Mascarenhasd, T., Natal Jorge, R.M., Ferreirae, A., Doblaré, M., Calvo, B.: Mechanical characterization of the softening behavior of human vaginal tissue. J. Mech. Beh. Biomed. Mater. **4**, 275–283 (2011)
50. Peña, E., Doblaré, M.: An anisotropic pseudo-elastic approach for modelling Mullins effect in fibrous biological materials. Mech. Res. Comm. **36**, 784–790 (2009)
51. Machado, G., Chagnon, G., Favier, D.: Induced anisotropy by the Mullins effect in filled silicone rubber. Mech. Mater. **50**, 70–80 (2012)
52. Kaliske, M.: A formulation of elasticity and viscoelasticity for fibre reinforced material at small and finite strains. Comput. Methods Appl. Mech. Eng. **185**, 225–243 (2000)
53. Govindjee, S., Simo, J.C.: Mullins' effect and the strain amplitude dependence of the storage modulus. Int. J. Solids. Struct. **29**, 1737–1751 (1992)
54. Bazant, Z.P., Oh, B.H.: Efficient numerical integration on the surface of a sphere. Z. Angew. Math. Mech. **66**, 37–49 (1986)
55. Zuñiga, A.E., Beatty, M.F.: A new phenomenological model for stress-softening in elastomers. Z. Angew. Math. Mech. **53**, 794–814 (2002)
56. Coleman, B.D., Gurtin, M.E.: Thermodynamics with internal state variables. J. Chem. Phys. **47**, 597–613 (1967)
57. Schröder, J., Neff, P., Balzani, D.: A variational approach for materially stable anisotropic hyperelasticity. Int. J. Solids. Struct. **42**, 4352–4371 (2005)

58. Li, D., Robertson, A.M.: A structural multi-mechanism constitutive equation for cerebral arterial tissue. Int. J. Solids Struct. **46**, 2920–2928 (2009)
59. Ehret, A.E., Itskov, M.: Modeling of anisotropic softening phenomena: Application to soft biological tissues. Int. J. Plast. **25**, 901–919 (2009)
60. Peña, E.: Prediction of the softening and damage effects with permanent set in fibrous biological materials. J. Mech. Phys. Solids **59**, 1808–1822 (2011)
61. Demiray, H.: A note on the elasticity of soft biological tissues. J. Biomech. **5**, 309–311 (1972)
62. Delfino, A., Stergiopulos, N., Moore, J.E. Jr., Meister, J.J.: Residual strain effects on the stress field in a thick wall finite element model of the human carotid bifurcation. J. Biomech. **30**, 777–786 (1997)
63. Holzapfel, G.A., Gasser, T.C., Ogden, R.W.: A new constitutive framework for arterial wall mechanics and a comparative study of material models. J. Elast. **61**, 1–48 (2000)